Control Engineering Practice 17 (2009) 1255–1264

Contents lists available at ScienceDirect

Control Engineering Practice

journal homepage: www.elsevier.com/locate/conengprac

Estimation of vehicle sideslip, tire force and wheel cornering stiffness

Guillaume Baffet [a,*], Ali Charara [a], Daniel Lechner [b]

[a] HEUDIASYC Laboratory, UMR CNRS 6599, Université de Technologie de Compiègne, Centre de recherche Royallieu, BP20529, 60205 Compiègne, France
[b] INRETS-MA Laboratory, Department of Accident Mechanism Analysis, Chemin de la Croix Blanche, 13300 Salon de Provence, France

ARTICLE INFO

Article history:
Received 26 July 2007
Accepted 27 May 2009
Available online 21 June 2009

Keywords:
Vehicle dynamics
Tire–road force
Sideslip angle
Cornering stiffness
Sliding-mode observer

ABSTRACT

This paper presents a process for the estimation of tire–road forces, vehicle sideslip angle and wheel cornering stiffness. The method uses measurements (yaw rate, longitudinal/lateral accelerations, steering angle and angular wheel velocities) only from sensors which can be integrated or have already been integrated in modern cars. The estimation process is based on two blocks in series: the first block contains a sliding-mode observer whose principal role is to calculate tire–road forces, while in the second block an extended Kalman filter estimates sideslip angle and cornering stiffness. More specifically, this study proposes an adaptive tire-force model that takes variations in road friction into account. The paper also presents a study of convergence for the sliding-mode observer. The estimation process was applied and compared to real experimental data, in particular wheel force measurements. The vehicle mass is assumed to be known. Experimental results show the accuracy and potential of the estimation process.

1. Introduction

Knowledge of vehicle variables such as tire forces and sideslip angle is essential for improving car safety, handling characteristics and comfort. Active safety systems such as anti-lock braking systems and electronic stability programs can significantly reduce the number of road accidents, and these safety systems may be improved if the variables of a car are well known. For instance, information about road friction means a better definition of potential trajectories, and therefore a better management of vehicle controls. However for both technical and economical reasons some fundamental data (such as tire forces, sideslip angle, road friction) are not measurable in a standard car. As a consequence, tire forces and sideslip angle must be observed or estimated. Fig. 1 illustrates wheel dynamic variables. The wheel sideslip angle represents the angular direction of the linear wheel velocity relative to the longitudinal wheel axis.

Vehicle-dynamic estimation has been widely discussed in the literature, e.g. (Arndt & Karidas, 2006; Gustafsson, 1997; Hsu & Gerdes, 2006; Kim, 2009; Lakehal-ayat, Tseng, Mao, & Karidas, 2006; Ono et al., 2003; Stephant, Charara, & Meizel, 2007; Tanelli, Savaresi, & Cantoni, 2006; Wesemeier & Isermann, 2009). The modeling of vehicle–road systems is complex because the vehicle trajectory depends on a wide variety of parameters, including tire, car and road properties. In the literature, the vehicle–road system is usually modeled by combining a vehicle model with a tire-force model (Baffet, Stephant, & Charara, 2007; Lechner, 2002; Ungoren, Peng, & Tseng, 2004). In this study, the estimation process is separated into two blocks (Fig. 2), where block 1 corresponds to the car body dynamic and block 2 corresponds to the tire–road interface dynamic.

The first block contains a sliding-mode observer (SMO) which estimates tire forces and yaw rate. This observer is constructed with a single-track model (Segel, 1956), in which forces are modeled without tire–road parameters ($\dot{F}_x = 0$, $\dot{F}_y = 0$). One advantage of this formulation is that the estimates will not be influenced by tire–road parameters.

In the second block an extended Kalman filter (EKF) supplies estimations of sideslip angle and wheel cornering stiffnesses. This observer is developed from a sideslip angle model and a linear adaptive tire-force model. The linear adaptive force model is proposed with an eye to correcting errors resulting from road friction changes.

By separating the estimation process in two blocks, the force estimates, in the first block, are not functions of road friction parameters. Consequently the first observer is particularly robust with respect to road friction changes. Moreover, the process is separated in two blocks for practical and analysis reasons. In fact, the gains of the two observers are easier to adjust than the gains of one bigger observer combining the two observers.

The rest of the paper is organized as follows. Section 2 describes the modeling of the first block, presents the sliding-mode observer and shows experimental results for the estimates

* Corresponding author. Tel.: +33 344234645; fax: +33 344234477.
E-mail addresses: guillaumebaffet@gmail.com (G. Baffet), acharara@hds.utc.fr (A. Charara), daniel.lechner@inrets.fr (D. Lechner).

0967-0661/$ - see front matter © 2009 Elsevier Ltd. All rights reserved.
doi:10.1016/j.conengprac.2009.05.005

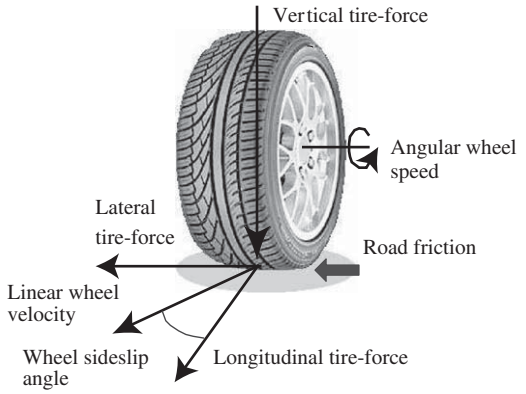

Fig. 1. Wheel dynamic variables.

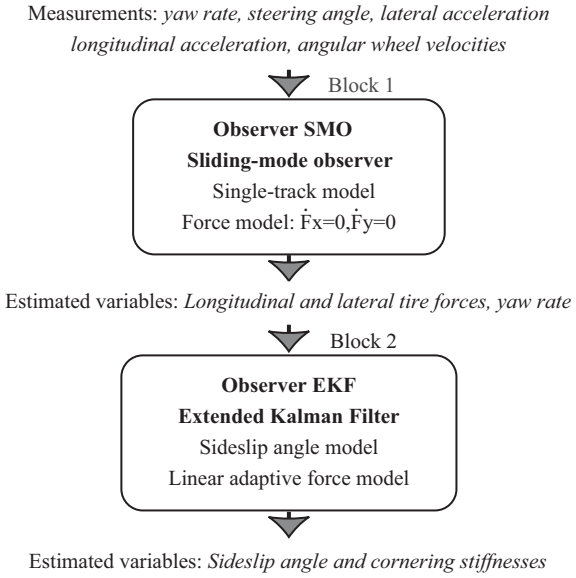

Fig. 2. The estimation process is divided into two blocks, where block 1 estimates the tire–road forces and block 2 calculates sideslip angle.

of tire forces. Section 3 describes the modeling of tire–road forces, proposes the extended Kalman filter, and presents experimental results performed within the second block. The two observers are evaluated with respect to sideslip angle and tire-force measurements. Section 4 describes the sensitivity to vehicle mass of the method. Section 5 presents the conclusion. Appendix A analyzes the convergence properties of the sliding-mode observer and Appendix B lists the different notations.

2. Tire–road force observer, SMO

2.1. Modeling of the sliding-mode observer

The observer SMO is based on the single-track model (Segel, 1956), which is currently used to describe vehicle-dynamic behavior (Kiencke & Daib, 1997). Fig. 3 presents the single-track model, where $\dot{\psi}$ is the yaw rate, γ_x and γ_y are the longitudinal and lateral accelerations, V_g is the vehicle velocity, β is the sideslip angle, δ is the steering angle, F_{yw1} and F_{yw2} are the front and rear lateral tire forces, F_{xw1} and F_{xw2} are the front and rear longitudinal tire forces, and F_{y1} and F_{x1} are the front lateral and longitudinal tire forces in the car body axis. L_1 and L_2 are the distances from the

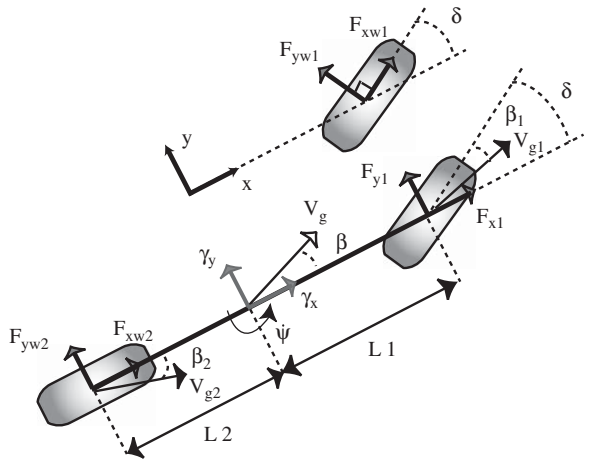

Fig. 3. The single-track model, also called the bicycle model, is used in the sliding-mode observer.

vehicle center of gravity to front and rear wheels, x and y are the longitudinal and lateral vehicle positions, V_{g1} and V_{g2} the front and the rear vehicle velocities, and β_1 and β_2 the front and rear sideslip angles.

Because of its simplicity, one advantage of the bicycle model is that time execution is sufficiently short for real time applications. However, this model ignores vehicle roll which has a large impact on the lateral acceleration, especially at high lateral accelerations.

In order to develop an observable system (notably in the case of null steering angle) (Nijmeijer & Van der Schaft, 1990), rear longitudinal tire force F_{xw2} is neglected relative to the front longitudinal force F_{x1} (assuming a front-wheel drive car in braking situation). The simplified equation for yaw acceleration can be formulated as the following dynamic relationship (single-track model):

$$\ddot{\psi} = \frac{1}{I_z}[L_1 F_{y1} - L_2 F_{yw2}], \tag{1}$$

where I_z is the yaw moment of inertia. The force evolutions and the measurements of the longitudinal and lateral accelerations are modeled as

$$\dot{F}_{y1} = 0, \quad \dot{F}_{yw2} = 0, \quad \dot{F}_{x1} = 0,$$
$$\gamma_y = \frac{F_{y1} + F_{y2}}{m}, \quad \gamma_x = \frac{F_{x1}}{m}, \tag{2}$$

where m is the vehicle mass. Consider the following state $\mathbf{X} \in \mathbf{R^4}$ and measurement $\mathbf{Y} \in \mathbf{R^3}$:

$$\mathbf{X} = [x_1, x_2, x_3, x_4] = [\dot{\psi}, F_{y1}, F_{yw2}, F_{x1}],$$
$$\mathbf{Y} = [y_1, y_2, y_3] = [\dot{\psi}, \gamma_y, \gamma_x]. \tag{3}$$

Vectors $\hat{\mathbf{x}} = [\hat{x}_1, \hat{x}_2, \hat{x}_3, \hat{x}_4]$ and $\hat{\mathbf{Y}} = [\hat{y}_1, \hat{y}_2, \hat{y}_3]$ represent the state estimates and the measurement estimates. The measurement model is

$$\hat{y}_1 = \hat{x}_1, \quad \hat{y}_2 = \frac{\hat{x}_2 + \hat{x}_3}{m}, \quad \hat{y}_3 = \frac{\hat{x}_4}{m}. \tag{4}$$

The estimation errors for states and measurements are denoted, respectively, as

$$\tilde{\mathbf{X}} = [\mathbf{X} - \hat{\mathbf{x}}] = [\tilde{x}_1, \tilde{x}_2, \tilde{x}_3, \tilde{x}_4], \quad \tilde{\mathbf{Y}} = [\mathbf{Y} - \hat{\mathbf{y}}] = [\tilde{y}_1, \tilde{y}_2, \tilde{y}_3]. \tag{5}$$

The observer SMO uses a sliding-mode structure based principally on the works of Drakunov and Utkin (1995), and Slotine, Hedrick, and Misawa (1987). The state estimates evolve according to the single-track model (1), the force model (2) and the sign of the

measurement estimation errors:

$$\begin{aligned}
\dot{\widehat{x}}_1 &= \frac{1}{I_z}[L_1\widehat{x}_2 - L_2\widehat{x}_3] + \Omega_1\,\mathrm{sign}(\widetilde{y}_1) + \Omega_2\,\mathrm{sign}(\widetilde{y}_2) + \Omega_3\,\mathrm{sign}(\widetilde{y}_3),\\
\dot{\widehat{x}}_2 &= \Omega_4\,\mathrm{sign}(\widetilde{y}_1) + \Omega_5\,\mathrm{sign}(\widetilde{y}_2) + \Omega_6\,\mathrm{sign}(\widetilde{y}_3),\\
\dot{\widehat{x}}_3 &= \Omega_7\,\mathrm{sign}(\widetilde{y}_1) + \Omega_8\,\mathrm{sign}(\widetilde{y}_2) + \Omega_9\,\mathrm{sign}(\widetilde{y}_3),\\
\dot{\widehat{x}}_4 &= \Omega_{10}\,\mathrm{sign}(\widetilde{y}_1) + \Omega_{11}\,\mathrm{sign}(\widetilde{y}_2) + \Omega_{12}\,\mathrm{sign}(\widetilde{y}_3),
\end{aligned} \tag{6}$$

where $\Omega_1,\ldots,\Omega_{12}$ are the observer gains. The convergence analysis of SMO is described in Appendix A. Choosing the observer gains such that

$$\begin{aligned}
&\{\Omega_2,\Omega_3,\Omega_6,\Omega_9,\Omega_{10},\Omega_{11}\} = 0,\\
&\{\Omega_1,\Omega_4,\Omega_5,\Omega_8,\Omega_{12}\} > 0,\\
&\Omega_7 < 0, \quad \Omega_4 = -\Omega_7, \quad \Omega_5 = \frac{L_2}{L_1}\Omega_8
\end{aligned} \tag{7}$$

implies the convergence of the estimation vector $\widehat{x}$ toward the system state X. In the experimental tests the gains were set as

$$\begin{aligned}
&\Omega_1 = 10, \quad \Omega_4 = 40\,000, \quad \Omega_5 = 52\,000, \quad \Omega_7 = -40\,000,\\
&\Omega_8 = 40\,000, \quad \Omega_{12} = 50\,000.
\end{aligned}$$

These gain values are chosen empirically, according to (7), numerous experimental tests and in order that the estimates converge quickly to the states. The sampling frequency is 100 Hz, and the chattering is avoided by using a linear function (Levant, 1993).

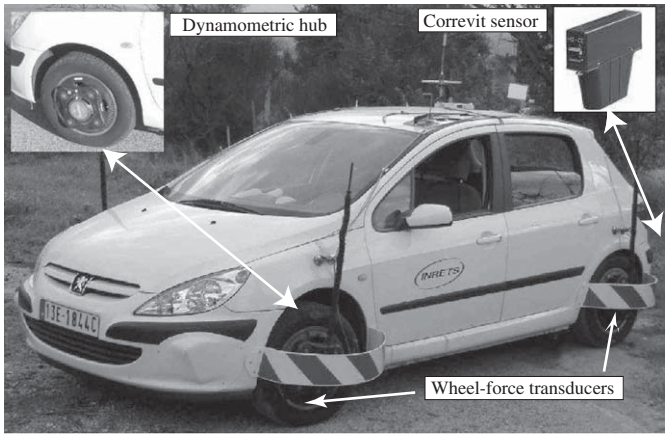

Fig. 4. INRETS MA Laboratory's experimental vehicle. Dynamometric hubs: wheel-force transducers. Correvit sensors: sideslip angle and velocity transducers.

2.2. Experimental results—observer SMO

The INRETS MA vehicle (see Fig. 4) is a Peugeot 307 equipped with a number of sensors including centimetric GPS, accelerometers, odometers, gyrometers, steering angle, three Correvits and four dynamometric hubs. The three Correvits (non-contact optical sensor) gives measurements of the sideslip angles and velocities of the vehicle rear, the front-right wheel and the rear-right wheel. The dynamometric hubs are placed at the four wheels and provide measurements of tire forces and wheel torques.

This study included two experimental tests: a slalom and a roundabout. These tests are representative of both longitudinal and lateral dynamic behaviors. The vehicle trajectories and the acceleration diagrams are shown in Figs. 5 and 6.

These experimental tests were performed in dry asphalt. During the first test (slalom), the vehicle first accelerated up to $\gamma_x = 0.3g$ (situation 1), then negotiated a slalom ($-0.6g < \gamma_y < 0.6g$, situation 2), before finally decelerating to $\gamma_x \approx -0.5g$ (situation 3). In the second test the vehicle negotiated a roundabout at maximum steering angle of 11°. The two diagrams show that the vehicle is subject to lateral accelerations lower than $0.7g$.

The estimation results are presented in two formats: as numerical estimation results compared with measurements, and as tables of normalized errors. The normalized error ε_z for an estimation z is defined as

$$\varepsilon_z(i) = \frac{100 \cdot |z(i) - z_{meas}(i)|}{\max|z_{meas}(i)|}. \tag{8}$$

This quantity is calculated for each sample. The vehicle parameters are $I_z = 3000\,\mathrm{kg\,m^{-2}}$, $L_1 = 1.12\,\mathrm{m}$, $L_2 = 1.46\,\mathrm{m}$, $m = 1447\,\mathrm{kg}$. The estimates of the tire forces along the wheel axis are obtained by applying the following equations:

$$F_{xw1} = F_{x1}\cos(\delta) + F_{y1}\sin(\delta), \quad F_{yw1} = F_{y1}\cos(\delta) - F_{x1}\sin(\delta). \tag{9}$$

Figs. 7 and 8, Tables 1 and 2 present SMO results for the two tests. These tables show the mean and the standard deviation of the normalized errors. The state estimates were initialized with the maximum measurements during the test (for instance $\widehat{x}_2(t=0) = 5448\,\mathrm{N}$ in the slalom test). In spite of these initializations the estimates converge quickly to the measurements, showing the good convergence properties of the observer.

Moreover, the SMO observer produces satisfactory estimates close to measurements for the two tests (normalized mean errors and standard deviation less than 6% in Tables 1 and 2). These good experimental results confirm that the observer approach may be appropriate for the estimation of tire forces.

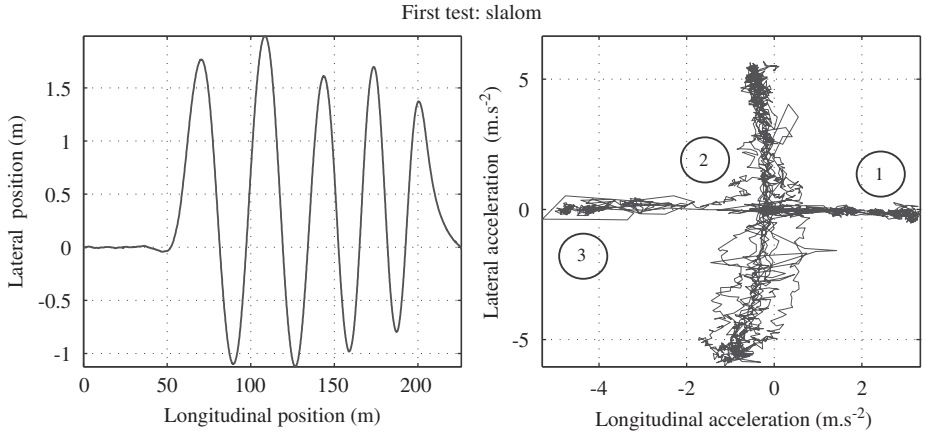

Fig. 5. Slalom experimental test, vehicle position, acceleration diagram.

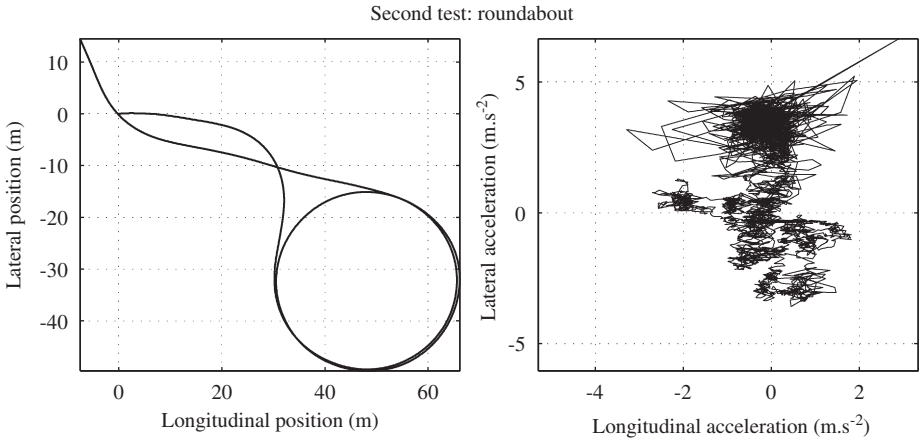

Fig. 6. Roundabout experimental test, vehicle position, acceleration diagram.

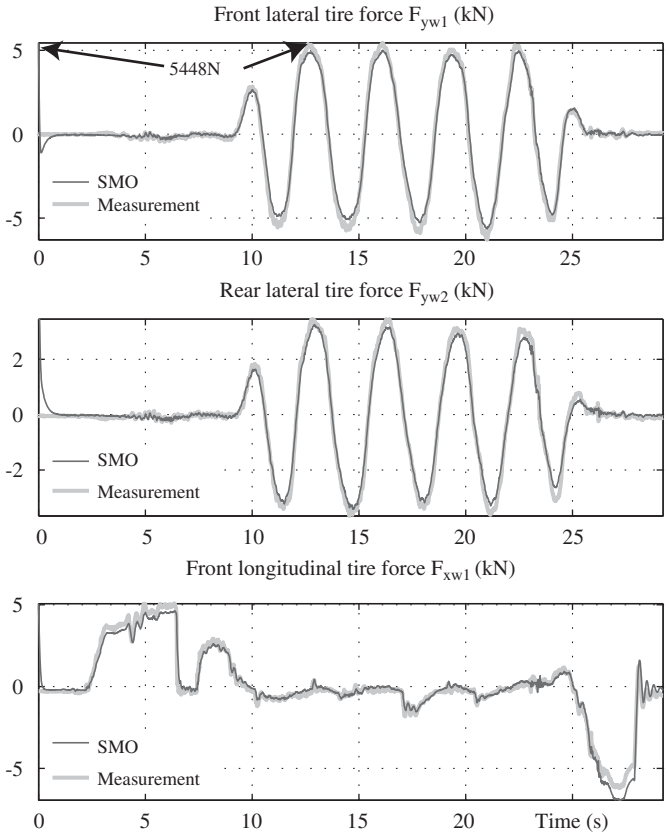

Fig. 7. Slalom test. SMO observer. Tire force estimates.

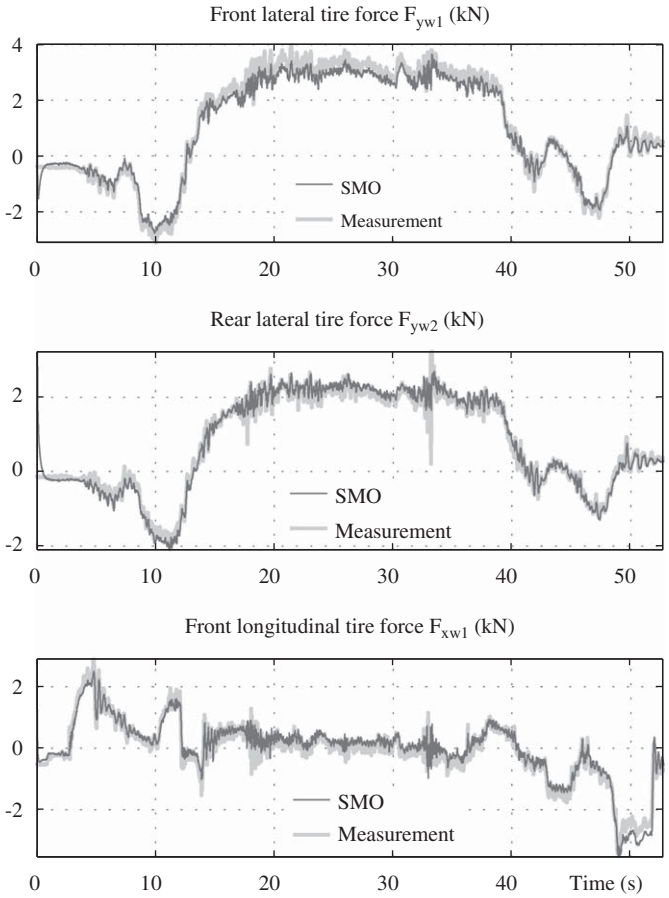

Fig. 8. Roundabout. SMO observer. Tire force estimates.

3. Sideslip angle and wheel cornering stiffness observer, EKF

This section introduces tire-force modeling and presents the observer EKF for the estimation of sideslip angle and wheel cornering stiffness. The filter EKF is constructed by combining models characterizing the vehicle sideslip angle and the tire–road contact forces. The sideslip angle evolution is formulated by using the single-track model (Segel, 1956):

$$\dot{\beta} = \frac{1}{mV_g}[F_{xw1}\sin(\delta-\beta) + F_{yw1}\cos(\delta-\beta) + F_{yw2}\cos(\beta)] - \dot{\psi}. \quad (10)$$

The wheel sideslip angles and the center of gravity sideslip angle are linked with the following relationships:

$$\beta_1 = \delta - \beta - \frac{L_1\dot{\psi}}{V_g}, \quad \beta_2 = -\beta + \frac{L_2\dot{\psi}}{V_g}. \quad (11)$$

The tire forces are usually modeled as a function of slips between tire and road, such as the wheel longitudinal slip and the wheel sideslip angle (Burckhardt, 1993; Canudas-De-Wit, Tsiotras, Velenis, Basset, & Gissinger, 2003; Pacejka & Bakker, 1991). Fig. 9 illustrates different lateral tire-force models (linear, linear

Table 1
Slalom test, SMO observer, maximum absolute values, normalized mean errors and standard deviation (Std).

Slalom	$\max\|z_{meas}\|$	$mean(\varepsilon_z)$ (%)	$std(\varepsilon_z)$ (%)
F_{y1}	6282 N	4.1	3.8
F_{y2}	3663 N	2.2	1.9
F_{x1}	6181 N	3.8	3.6
$\dot{\psi}$	33.6°/s	0.5	0.3

Table 2
Roundabout test, SMO observer, maximum absolute values, normalized mean errors and standard deviation (Std).

Roundabout	$\max\|z_{meas}\|$	$mean(\varepsilon_z)$ (%)	$std(\varepsilon_z)$ (%)
F_{y1}	4010 N	5.2	3.4
F_{y2}	3215 N	3.7	3.2
F_{x1}	3434 N	4.8	3.9
$\dot{\psi}$	23.0°/s	0.2	0.2

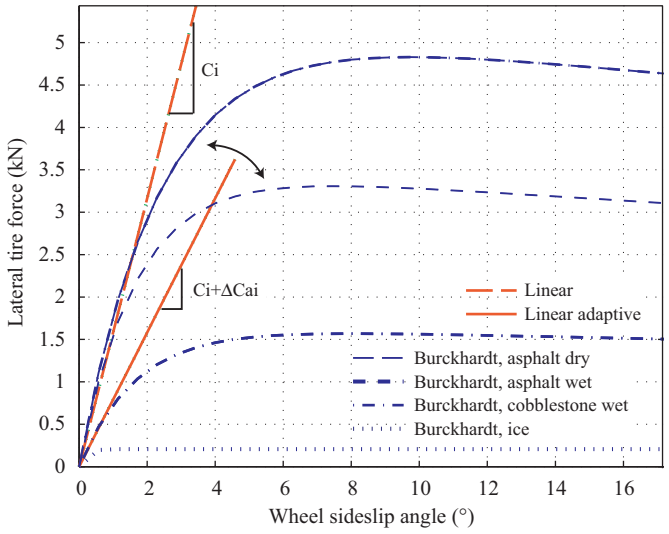

Fig. 9. Lateral tire-force models: linear, linear adaptive, Burckhardt for various road surfaces.

adaptive and Burckhardt for various road surfaces, Kiencke & Nielsen, 2000).

For normal driving situations, lateral tire forces are usually considered linear with respect to sideslip angle (linear model, cumulative lateral tire-force for each axle):

$$F_{ywi}(\beta_i) = C_i\beta_i, \quad i = 1,2, \tag{12}$$

where C_i is the wheel cornering stiffness (a parameter closely related to tire–road friction).

When road friction changes or when the nonlinear tire domain is reached, wheel cornering stiffness varies. Some studies have described observers which take cornering stiffness (or road friction) variations into account (Rabhi, M'Sirdi, Zbiri, & Delanne, 2005; Ray, 1997). In Rabhi et al. (2005) tire–road parameters are identified with a sliding-mode observer, while in Ray (1997) tire–road forces are modeled with an integrated random walk model ($\ddot{F} = 0$).

In this study, an adaptive tire-force model is proposed (hereafter termed the "linear adaptive force model"). This model is based on the linear model to which a readjustment variable ΔC_{ai} has been added to correct wheel cornering stiffness errors (Fig. 9):

$$F_{ywi}(\beta_i) = (C_i + \Delta C_{ai})\beta_i, \quad i = 1,2. \tag{13}$$

The variable ΔC_{ai} is included in the state vector of the EKF observer and its evolution equation is formulated according to the model ($\Delta\dot{C}_{ai} = 0$).

The EKF observer is constructed with state $\mathbf{X}' \in \mathbf{R^3}$, input $\mathbf{U}' \in \mathbf{R^4}$ and measurement $\mathbf{Y}' \in \mathbf{R^3}$ as

$$\begin{aligned}
&\mathbf{X}' = [x_1', x_2', x_3'] = [\beta, \Delta C_{a1}, \Delta C_{a2}],\\
&\mathbf{U}' = [u_1', u_2', u_3', u_4'] = [\delta, \dot{\psi}, V_g, F_{xw1}],\\
&\mathbf{Y}' = [y_1', y_2', y_3'] = [F_{yw1}, F_{yw2}, \gamma_y].
\end{aligned} \tag{14}$$

The measurement model is

$$\begin{aligned}
&y_1' = (C_1 + x_2')\beta_1, \quad y_2' = (C_2 + x_3')\beta_2,\\
&y_3' = \frac{1}{m}[(C_1 + x_2')\beta_1\cos(u_1') + (C_2 + x_3')\beta_2 + u_4'\sin(u_1')].
\end{aligned} \tag{15}$$

Consider the state estimates denoted as $\hat{x}' = [\hat{x}_1', \hat{x}_2', \hat{x}_3']$. The state evolution model of EKF is

$$\begin{aligned}
&\dot{\hat{x}}_1' = \frac{u_4'\sin(u_1' - \hat{x}_1') + F_{auxi1}\cos(u_1' - \hat{x}_1') + F_{auxi2}\cos(\hat{x}_1')}{mu_3'} - u_2',\\
&\dot{\hat{x}}_2' = 0, \quad \dot{\hat{x}}_3' = 0,
\end{aligned} \tag{16}$$

where the auxiliary variables F_{auxi1} and F_{auxi2} are calculated as

$$\begin{aligned}
&F_{auxi1} = (C_1 + \hat{x}_2')\left(u_1' - \hat{x}_1' - \frac{L_1u_2'}{u_3'}\right),\\
&F_{auxi2} = (C_2 + \hat{x}_3')\left(-\hat{x}_1' + \frac{L_2u_2'}{u_3'}\right).
\end{aligned} \tag{17}$$

The extended Kalman filter is based on a study by Kalman (1960) and constructed according to an algorithm proposed in Mohinder and Angus (1993). The EKF algorithm is set according to noise variance–covariance matrices. These matrices, denoted as $\mathbf{Q_s}$, $\mathbf{Q_e}$ and $\mathbf{Q_m}$, are associated, respectively, to the noises of the measurements, the inputs and the models. These noises are assumed to be Gaussian, white and centered. The variance–covariance matrices are set according to the vehicle state. This is explained with Figs. 10 and 11.

Fig. 10 presents the measurements of the front lateral tire forces F_{y1} as a function of the front wheel sideslip angles β_1 (for a slalom test). Fig. 11 illustrates straight lines representing different potential cornering stiffnesses estimates ($C_i + \Delta C_{ai} = F_{yi}/\beta_i$). Neglecting the force saturation, the estimation of cornering stiffness is not adapted in four zones:

- in zones 1 and 2: when $\beta_i * F_{yi} < 0$ (not adapted because the cornering stiffness must be positive) and
- in zones 3 and 4: when the lateral dynamic is low: $F_{yi} < \lambda_i$ (threshold), because some ratios F_{yij}/β_{ij} may have very different values in these zones.

The variance–covariance matrices ($\mathbf{Q_s}$, $\mathbf{Q_m}$) are set in order that the cornering stiffness estimation is performed mainly in zones 5 and 6.

The variance–covariance matrices are set

- in zones 1–4:
  $\mathbf{Q}_s = \mathrm{diag}[1e, 1e6, 1e6]$,
  $\mathbf{Q}_m = \mathrm{diag}[1e-13, 0, 0]$,
- in zones 5, 6:
  $\mathbf{Q}_s = \mathrm{diag}[0.1, 0.1, 0.1]$,
  $\mathbf{Q}_m = \mathrm{diag}[1e-13, 0.24, 0.24]$.

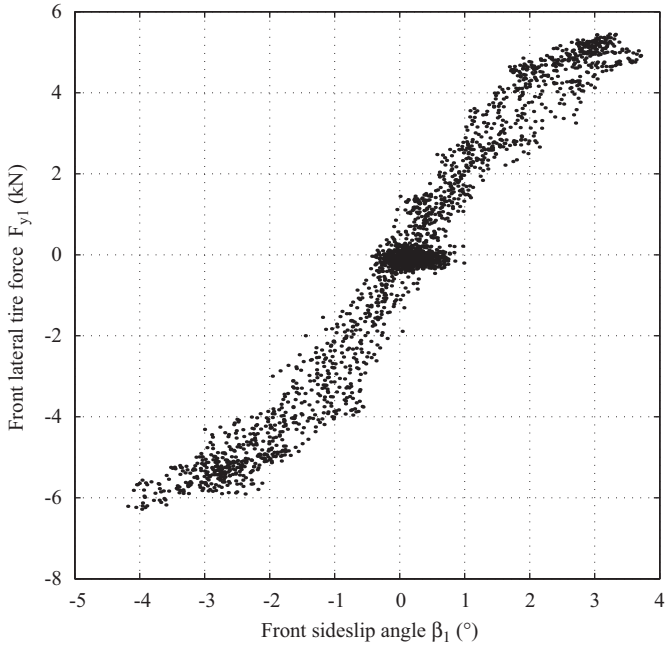

Fig. 10. Experimental test measurements of the front lateral tire forces as a function of the front-wheel sideslip angles.

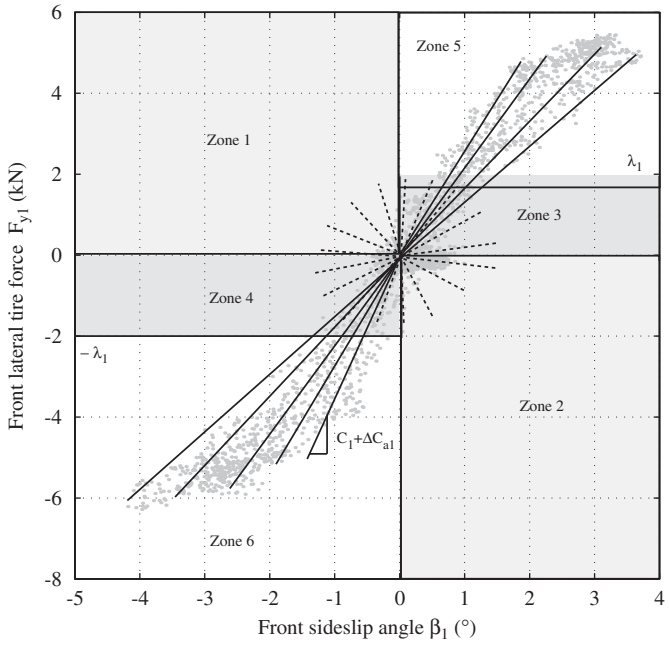

Fig. 11. Experimental test measurements of the front lateral tire forces as a function of the front-wheel sideslip angles. The straight lines represent different cornering stiffnesses ($C_i + \Delta C_{ai} = F_{yij}/\beta_{ij}$). State zones 1, 2, 3 and 4 are not adapted for the estimation of cornering stiffness. The observer EKF mainly corrects cornering stiffness in zones 5 and 6.

An observability function was calculated using a Lie derivative method (Nijmeijer & Van der Schaft, 1990). The rank of the observability function, which was calculated along experimental trajectories, corresponded to the state vector dimension (3), and consequently system EKF was locally observable.

3.1. Experimental results—observer EKF

In order to demonstrate the improvement provided by the observer using the linear adaptive force model (13), another observer constructed with a linear force model (12) was used in comparison (observer denoted ORL). The robustness of the two observers was tested with respect to tire–road friction variations by performing the tests with different cornering stiffness parameters ($[C_1, C_2] * 0.5, 1, 1.5$ with $C_1 = 65\,000\,\mathrm{N\,rad^{-1}}$ and $C_2 = 50\,000\,\mathrm{N\,rad^{-1}}$). The different observers were evaluated for the two tests presented in Section 2.2.

Figs. 12 and 13 show the results for the ORL observer (using the linear force model) when estimating rear sideslip angle. The ORL observer gives good results when cornering stiffnesses are approximately known ($[C_1, C_2] * 1$). However, this observer is not robust when cornering stiffnesses change ($[C_1, C_2] * 0.5, 1.5$). When cornering stiffness is reduced ORL overestimates rear sideslip angle (in absolute value) and, conversely, when cornering stiffness is increased rear sideslip angle is overestimated.

Figs. 14 and 15, Tables 3 and 4 present rear sideslip angle estimation results obtained with the adaptive observer EKF for the two tests. The performance robustness of EKF is satisfactory since rear sideslip angle is well estimated and similar irrespective of cornering stiffness settings. This result is confirmed by the EKF normalized errors (Tables 3 and 4) which are approximately similar.

Figs. 16 and 17 present the front and rear cornering stiffness estimates ($C_i + \Delta C_i$). It can be seen that the cornering stiffness estimates remain approximately constant when the lateral

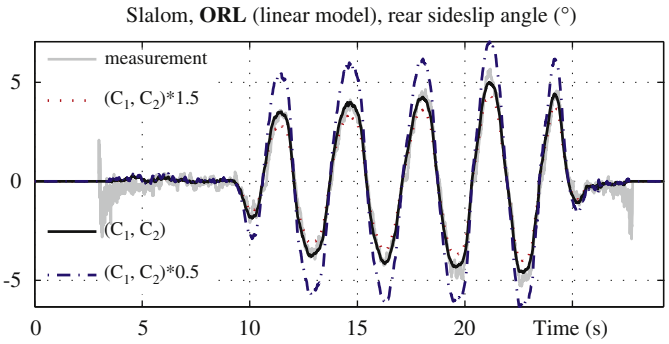

Fig. 12. *ORL observer* (*linear tire-force model*), rear sideslip angle estimates, with different stiffness settings.

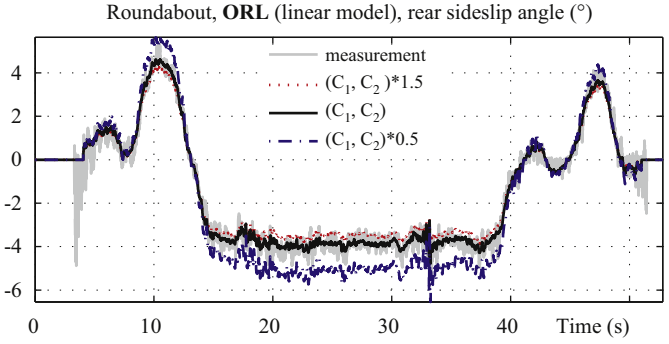

Fig. 13. *ORL observer* (*linear tire-force model*), rear sideslip angle estimates, with different stiffness settings.

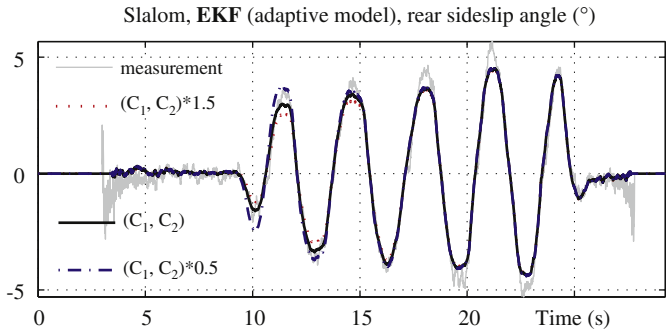

Fig. 14. Slalom test, *EKF observer* (*linear adaptive force model*), with different cornering stiffness settings. Rear sideslip angle estimates.

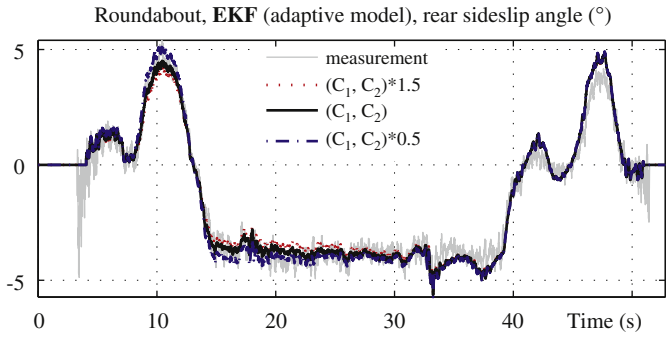

Fig. 15. Slalom test, *EKF observer* (*linear adaptive force model*), with different cornering stiffness settings. Rear sideslip angle estimates.

Table 3
Slalom test, EKF observer, maximum absolute values, normalized mean errors and standard deviation (Std) of the rear sideslip angle.

Slalom	$(C_1, C_2) * 0.5$	(C_1, C_2)	$(C_1, C_2) * 1.5$
$\max\lvert\beta_2\rvert$ (deg)	5.7	5.7	5.7
mean(ε_z) (%)	5.0	4.4	5.1
std(ε_z) (%)	5.9	5.2	5.5

Table 4
Roundabout test, EKF observer, maximum absolute values, normalized mean errors and standard deviation (Std) of the rear sideslip angle.

Roundabout	$(C_1, C_2) * 0.5$	(C_1, C_2)	$(C_1, C_2) * 1.5$
$\max\lvert\beta_2\rvert$ (deg)	5.4	5.4	5.4
mean(ε_z) (%)	8.1	6.4	5.9
std(ε_z) (%)	7.4	6.6	6.5

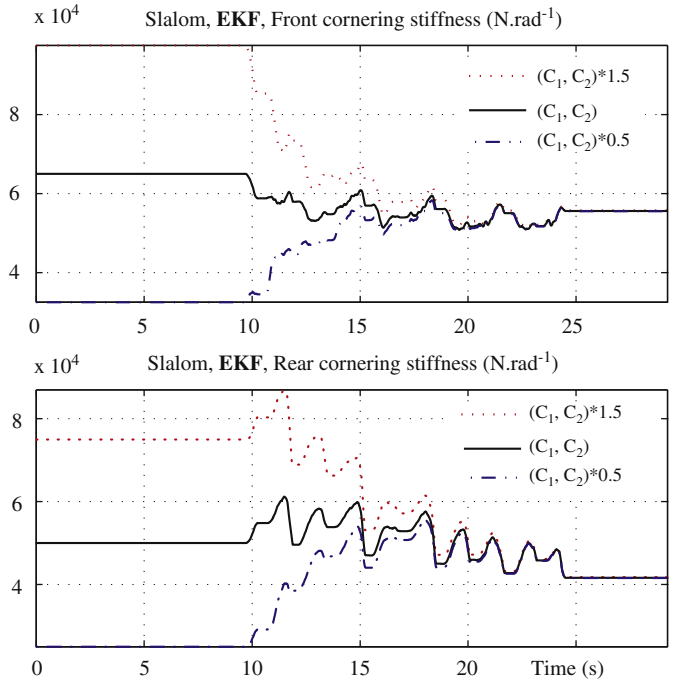

Fig. 16. Slalom test, *EKF observer* (*linear adaptive force model*), with different cornering stiffness settings $[(C_1, C_2) = (65\,000, 50\,000) * (0.5, 1, 1.5)\,\mathrm{N\,rad^{-1}}]$. Front and rear cornering stiffness estimates $C_i + \Delta C_{ai}$.

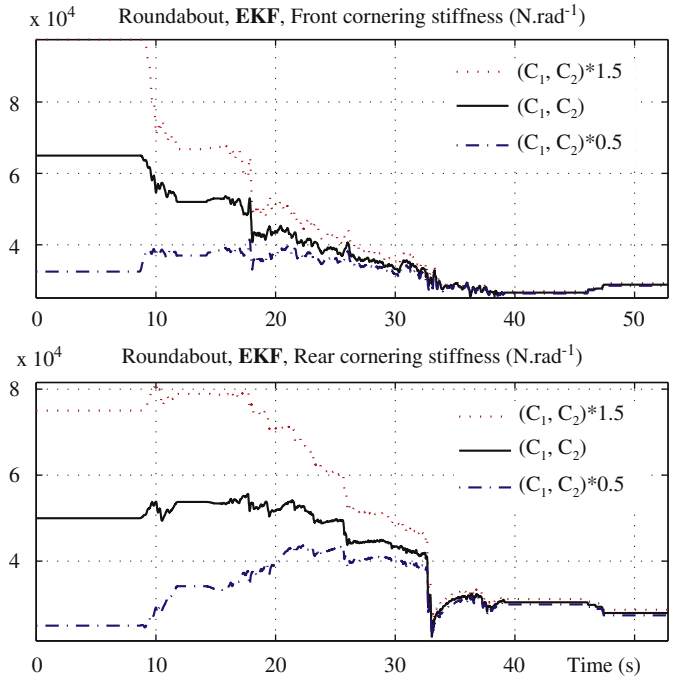

Fig. 17. Roundabout test, *EKF observer* (*linear adaptive force model*), with different cornering stiffness settings $[(C_1, C_2) = (65\,000, 50\,000) * (0.5, 1, 1.5)\,\mathrm{N\,rad^{-1}}]$. Front and rear cornering stiffness estimations $C_i + \Delta C_{ai}$.

dynamic (sideslip angles, lateral tire forces) is low, that is to say during the first 10 s in the case of the slalom, and the first 9 s in the case of the roundabout. Then, at the beginning of the slalom at 10 s or at the beginning of the roundabout at 9 s, the lateral dynamic becomes sufficiently large, and the estimates of the cornering stiffness converge quickly to the same values. The new information obtained from ΔC_{ai} may be used as an indication of the road friction. Indeed, for same values of the wheel sideslip angle, a significative change of ΔC_{ai} variable can indicate a road friction change (Baffet, 2007).

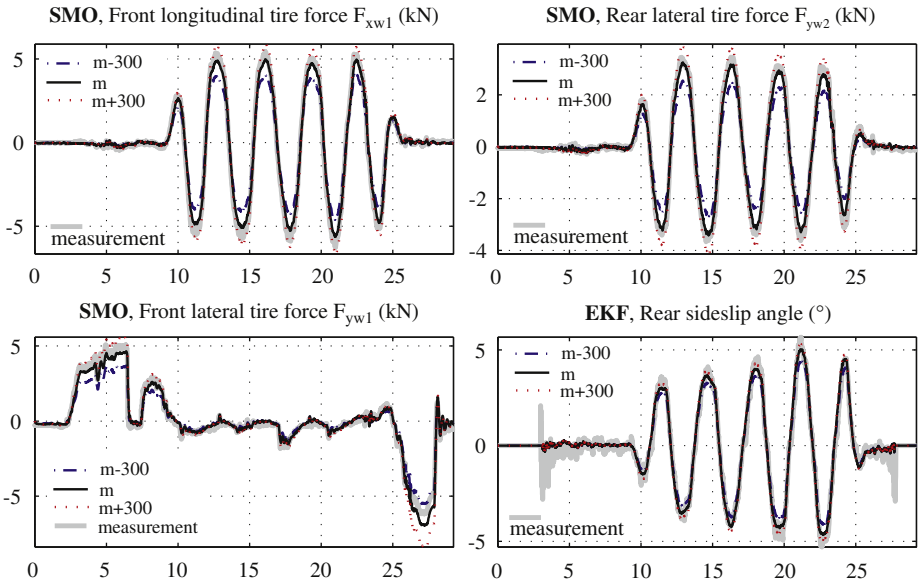

Fig. 18. Slalom test, with different mass settings: $m+300$ kg, $m=1447$ kg, $m-300$ kg.

4. Sensitivity to vehicle mass

As shown in Han, Kim, Jo, and Huh (2009), the mass can be estimated. This section presents the sensitivity of the estimation process when the vehicle mass is unknown. Three tests are performed with a different mass ($m=1447$ kg, $m+300$, $m-300$). Fig. 18 and Table 5 present the results. Concerning the tire forces, estimates increase when the mass parameter is increased (in absolute value), and conversely, estimates decrease when the mass is reduced. The tire force estimates converge to different values, showing that SMO is sensitive to changes in vehicle mass. As regards the rear sideslip angle, the variations induced by mass change are lower than those of the tire force estimates. This is confirmed by Table 5, where normalized mean errors of F_{y2} varies from 2.2% to 10.4%, whereas normalized mean errors of β_2 changes from 4.4% to 5.4%. This can be explained by regarding the sideslip angle model (10), where the mass change in the denominator is partially compensated for the force change in the numerator.

Table 5
Slalom test, robustness to vehicle mass ($m=1447$ kg). Maximum absolute values, normalized mean errors and standard deviation (Std).

Slalom	$m-300$ kg	m	$m+300$ kg
F_{y1}			
$\max\|z_{meas}\|$ (N)	6282	6282	6282
$mean(\varepsilon_z)$ (%)	8.0	4.1	4.9
$std(\varepsilon_z)$ (%)	8.2	3.8	4.8
F_{y2}			
$\max\|z_{meas}\|$ (N)	3663	3663	3663
$mean(\varepsilon_z)$ (%)	10.4	2.2	4.7
$std(\varepsilon_z)$ (%)	10.1	1.9	4.5
F_{x1}			
$\max\|z_{meas}\|$ (N)	6181	6181	6181
$mean(\varepsilon_z)$ (%)	5.9	3.8	5.5
$std(\varepsilon_z)$ (%)	5.9	3.6	8.1
β_2			
$\max\|z_{meas}\|$ (deg)	5.7	5.7	5.7
$mean(\varepsilon_z)$ (%)	5.4	4.4	5.1
$std(\varepsilon_z)$ (%)	5.8	5.2	5.7

5. Conclusion

This study deals with two vehicle-dynamic observers constructed for use in a two-block estimation process. The block 1 mainly estimates tire-forces (without an explicit tire-force model and a known vehicle mass), while block 2 calculates sideslip angle and corrects cornering stiffnesses (with an adaptive tire-force model).

The first observer SMO (block 1), a sliding-mode observer, was constructed by finding the gains with respect to the convergence. The experimental evaluations of SMO are satisfactory, showing estimates close to the measurements and good convergence properties.

The second observer EKF (block 2), an extended Kalman filter combined with an adaptive tire-force model, was evaluated for different cornering stiffness settings and was compared with an observer constructed with a fixed tire-force model (ORL). Results show that ORL is not robust when cornering stiffness parameters change, whereas EKF gives good estimates of the sideslip angle. This result justifies the use of an adaptive tire-force model.

The different results show the potential of the two-block estimation process. The first block has the advantage of providing satisfactory force estimates without a tire-force model, whereas the second block provides robust sideslip angle estimates with respect to cornering stiffness changes.

Acknowledgments

This work was supported by the PREDIT-SARI-RADARR program. The authors express gratefulness for the reviewer inputs that improve readability and proof of the sliding-mode observer.

Appendix A. Convergence of the SMO observer

The aim is to set gains $\Omega_1,\ldots,\Omega_{12}$ which lead to the state estimation errors $\tilde{X}$ converging toward 0. The evolution equations for the state estimation errors are the following:

$$\begin{aligned}
&\dot{\tilde{\mathbf{X}}} = \dot{\mathbf{X}} - \dot{\hat{\mathbf{x}}},\\
&\dot{\tilde{x}}_1 = \frac{1}{I_z}[L_1\tilde{x}_2 - L_2\tilde{x}_3] - \Omega_1\,\mathrm{sign}(\tilde{y}_1) - \Omega_2\,\mathrm{sign}(\tilde{y}_2) - \Omega_3\,\mathrm{sign}(\tilde{y}_3),\\
&\dot{\tilde{x}}_2 = -\Omega_4\,\mathrm{sign}(\tilde{y}_1) - \Omega_5\,\mathrm{sign}(\tilde{y}_2) - \Omega_6\,\mathrm{sign}(\tilde{y}_3),\\
&\dot{\tilde{x}}_3 = -\Omega_7\,\mathrm{sign}(\tilde{y}_1) - \Omega_8\,\mathrm{sign}(\tilde{y}_2) - \Omega_9\,\mathrm{sign}(\tilde{y}_3),\\
&\dot{\tilde{x}}_4 = -\Omega_{10}\,\mathrm{sign}(\tilde{y}_1) - \Omega_{11}\,\mathrm{sign}(\tilde{y}_2) - \Omega_{12}\,\mathrm{sign}(\tilde{y}_3).
\end{aligned} \tag{A.1}$$

Proposition 1. *Consider the following Lyapunov functions* $(\Phi_1,\Phi_2,\Phi_3,\Phi_4)$:

$$\begin{aligned}
&\Phi_1 = \tfrac{1}{2}\tilde{x}_1^2, \quad \Phi_2 = \tfrac{1}{2}\tilde{x}_4^2, \quad \Phi_3 = \tfrac{1}{2}(\tilde{x}_2+\tilde{x}_3)^2,\\
&\Phi_4 = \tfrac{1}{2}(L_1\tilde{x}_2 - L_2\tilde{x}_3)^2.
\end{aligned} \tag{A.2}$$

If the derivatives of the Lyapunov functions are negative, then the estimates $\hat{\mathbf{x}}$ *will converge toward the system states* $\mathbf{X}$.

Proof 1. The Lyapunov functions $\Phi_1,\ldots,\Phi_4$ are positive along all state trajectories, and consequently if the derivatives $\dot{\Phi}_1,\ldots,\dot{\Phi}_4$ are negative, then the Lyapunov functions will converge toward zero. This entails the following convergence:

$$\tilde{x}_1 \longrightarrow 0, \quad \tilde{x}_4 \longrightarrow 0, \quad \tilde{x}_2+\tilde{x}_3 \longrightarrow 0, \quad L_1\tilde{x}_2 - L_2\tilde{x}_3 \longrightarrow 0 \tag{A.3}$$

and consequently: $\hat{x}_1 \longrightarrow x_1, \hat{x}_4 \longrightarrow x_4$. The convergence $\tilde{x}_2+\tilde{x}_3 \longrightarrow 0$ implies two possibilities at the switching surface:

- either $[\tilde{x}_2 \longrightarrow 0$ and $\tilde{x}_3 \longrightarrow 0]$, then $\hat{x}_2 \longrightarrow x_2$ and $\hat{x}_3 \longrightarrow x_3$ or
- $[\tilde{x}_2 \longrightarrow -\tilde{x}_3]$, then the convergence (A.3) implies $\tilde{x}_2(L_1+L_2) \longrightarrow 0$, this entails the convergence $\hat{x}_2 \longrightarrow x_2$ and $\hat{x}_3 \longrightarrow x_3$. □

Remark 1. The Lyapunov functions (A.2) correspond to the estimation errors for: yaw rate $\dot{\psi}$ (Φ_1), lateral acceleration γ_y (Φ_2), yaw acceleration $\ddot{\psi}$ (Φ_3), longitudinal acceleration γ_x (Φ_4). Gains $\Omega_1,\ldots,\Omega_{12}$ are chosen so as to make the Lyapunov function derivatives negative.

Proposition 2. *If the gains are selected such that*

$$\begin{aligned}
&\Omega_1 \geq |\Omega_2| + |\Omega_3| + \left|\frac{1}{I_z}(L_1\tilde{x}_2 + L_2\tilde{x}_3)\right| + \varepsilon,\\
&\Omega_{12} \geq |\Omega_{11}| + |\Omega_{10}| + \varepsilon,
\end{aligned} \tag{A.4}$$

where $\varepsilon>0$ *then the estimates of the yaw rate* $\hat{x}_1$ *and longitudinal tire force* $\hat{x}_4$ *converge toward the states* x_1 *and* x_4, *respectively.*

Proof 2a. The derivative of the Lyapunov function Φ_1 is

$$\dot{\Phi}_1 = \tilde{x}_1\dot{\tilde{x}}_1,$$

$$\dot{\Phi}_1 = \tilde{x}_1\left[\frac{1}{I_z}(L_1\tilde{x}_2 - L_2\tilde{x}_3) - \Omega_1\,\mathrm{sign}(\tilde{y}_1) - \Omega_2\,\mathrm{sign}(\tilde{y}_2) - \Omega_3\,\mathrm{sign}(\tilde{y}_3)\right],$$

$$\begin{aligned}
\dot{\Phi}_1 = &-\tilde{x}_1\Big[\Omega_1\,\mathrm{sign}(\tilde{x}_1) + \Omega_2\,\mathrm{sign}(\tilde{x}_2+\tilde{x}_3)\\
&+\Omega_3\,\mathrm{sign}(\tilde{x}_4) - \frac{1}{I_z}(L_1\tilde{x}_2 - L_2\tilde{x}_3)\Big].
\end{aligned} \tag{A.5}$$

Using the triangle inequality and (A.4) now gives the following inequality for the Lyapunov function:

$$\dot{\Phi}_1 \leq -\tilde{x}_1\varepsilon\,\mathrm{sign}(\tilde{x}_1) < 0.$$

This derivative is negative and Φ_1 is positive, and consequently this induces the convergence $\Phi_1 \longrightarrow 0$ $\tilde{x}_1 \longrightarrow 0$ and therefore $\hat{x}_1 \longrightarrow x_1$. □

Remark 2a. At the switching surface $\dot{\tilde{x}}_1 = 0$ this result implies

$$\mathrm{sign}_{eq}(\tilde{x}_1) = \frac{1}{\Omega_1 I_z}[L_1\tilde{x}_2 - L_2\tilde{x}_3]. \tag{A.6}$$

Proof 2b. The derivative of the Lyapunov function Φ_2 is

$$\begin{aligned}
\dot{\Phi}_2 &= \tilde{x}_4\dot{\tilde{x}}_4\\
&= \tilde{x}_4[-\Omega_{10}\,\mathrm{sign}(\tilde{y}_1) - \Omega_{11}\,\mathrm{sign}(\tilde{y}_2) - \Omega_{12}\,\mathrm{sign}(\tilde{y}_3)]\\
&= \tilde{x}_4[-\Omega_{10}\,\mathrm{sign}(\tilde{x}_1) - \Omega_{11}\,\mathrm{sign}(\tilde{x}_2+\tilde{x}_3) - \Omega_{12}\,\mathrm{sign}(\tilde{x}_4)].
\end{aligned} \tag{A.7}$$

Using the triangle inequality and (A.4) now gives the following inequality on the Lyapunov function Φ_2:

$$\dot{\Phi}_2 \leq -\tilde{x}_4\varepsilon\,\mathrm{sign}(\tilde{x}_4) < 0.$$

This derivative is negative and Φ_2 is positive, and consequently this implies the convergence $\Phi_2 \longrightarrow 0$, $\tilde{x}_4 \longrightarrow 0$ and therefore $\hat{x}_4 \longrightarrow x_4$. □

Proposition 3. *Choosing the gains such that*

$$\begin{aligned}
&\Omega_5 + \Omega_8 \geq |\Omega_6| + |\Omega_9| + \varepsilon,\\
&\Omega_4 = -\Omega_7 > 0,\\
&\Omega_5 = \Omega_8 L_2/L_1,
\end{aligned} \tag{A.8}$$

where $\varepsilon>0$, *implies convergence of lateral tire force estimates* $(\hat{x}_2,\hat{x}_3)$ *toward the states* (x_2,x_3).

Proof 3a. The derivative of the Lyapunov function Φ_3 is:

$$\begin{aligned}
\dot{\Phi}_3 &= (\tilde{x}_2+\tilde{x}_3)(\dot{\tilde{x}}_2+\dot{\tilde{x}}_3)\\
&= (\tilde{x}_2+\tilde{x}_3)[-(\Omega_4+\Omega_7)\,\mathrm{sign}(\tilde{y}_1) - (\Omega_5+\Omega_8)\,\mathrm{sign}(\tilde{y}_2)\\
&\quad - (\Omega_6+\Omega_9)\,\mathrm{sign}(\tilde{y}_3)].
\end{aligned} \tag{A.9}$$

Using (A.8) and the triangle inequality yields the following inequality:

$$\dot{\Phi}_3 \leq -(\tilde{x}_2+\tilde{x}_3)\varepsilon\,\mathrm{sign}(\tilde{x}_2+\tilde{x}_3) < 0.$$

Consequently, with Φ_3 positive this implies convergences $\Phi_3 \longrightarrow 0$ and $\tilde{x}_2+\tilde{x}_3 \longrightarrow 0$.

Proof 3b. The derivative calculation of Lyapunov function Φ_4 gives

$$\begin{aligned}
&\dot{\Phi}_4 = (L_1\tilde{x}_2 - L_2\tilde{x}_3)(L_1\dot{\tilde{x}}_2 - L_2\dot{\tilde{x}}_3),\\
&\dot{\Phi}_4 = (L_1\tilde{x}_2 - L_2\tilde{x}_3)[(-L_1\Omega_4 + L_2\Omega_7)\,\mathrm{sign}(\tilde{y}_1)\\
&\qquad + (-L_1\Omega_5 + L_2\Omega_8)\,\mathrm{sign}(\tilde{y}_2)].
\end{aligned} \tag{A.10}$$

Applying the result (A.6) and choosing $\Omega_4 = -\Omega_7$, (A.10) becomes

$$\begin{aligned}
\dot{\Phi}_4 = (L_1\tilde{x}_2 - L_2\tilde{x}_3)\Big[&\frac{\Omega_7}{\Omega_1 I_z}(L_1+L_2)(L_1\tilde{x}_2 - L_2\tilde{x}_3)\\
&+ (-L_1\Omega_5 + L_2\Omega_8)\,\mathrm{sign}(\tilde{y}_2)\Big].
\end{aligned} \tag{A.11}$$

Specifying $\Omega_5 = \Omega_8 L_2/L_1$ and $\Omega_7<0$ means that the derivative

$$\dot{\Phi}_4 = \frac{\Omega_7(L_1+L_2)}{\Omega_1 I_z}(L_1\tilde{x}_2 - L_2\tilde{x}_3)^2 < 0 \tag{A.12}$$

becomes negative, which implies the convergences $\Phi_4 \longrightarrow 0$, and therefore $L_1\tilde{x}_2 - L_2\tilde{x}_3 \longrightarrow 0$. Moreover, $\tilde{x}_2+\tilde{x}_3 \longrightarrow 0$, consequently this induces the convergence $(\tilde{x}_2,\tilde{x}_3) \longrightarrow (x_2,x_3)$. □

Appendix B. Nomenclature

Tables B1 and B2 present the different notations.

Table B1
Nomenclature (first part).

Symbol	Description
C_1	Front cornering stiffness ($N\,rad^{-1}$)
C_2	Rear cornering stiffness ($N\,rad^{-1}$)
F_{x1}	Front longitudinal tire force (in body car axis) (N)
F_{y1}	Front lateral tire force (in body car axis) (N)
F_{xw1}	Front longitudinal tire force (in wheel axis) (N)
F_{xw2}	Rear longitudinal tire force (in wheel axis) (N)
F_{yw1}	Front lateral tire force (in wheel axis) (N)
F_{yw2}	Rear lateral tire force (in wheel axis) (N)
$\Omega_1, \ldots, \Omega_{20}$	SMO sliding-mode observer gains
I_z	Yaw moment of inertia ($kg\,m^{-2}$)
L_1	Center of gravity to front axle distance (m)
L_2	Center of gravity to rear axle distance (m)
m	Vehicle mass (kg)
$\mathbf{Q_e}$	Variance–covariance matrix for input noises
$\mathbf{Q_m}$	Variance–covariance matrix for model noises
$\mathbf{Q_s}$	Variance–covariance matrix for measurement noises
$\Phi_1, \ldots, \Phi_5$	Lyapunov functions
V_g	Center of gravity vehicle speed ($m\,s^{-1}$)
V_{g1}	Front vehicle speed ($m\,s^{-1}$)
V_{g2}	Rear vehicle speed ($m\,s^{-1}$)
β	Center of gravity sideslip angle (rad)
β_1	Front sideslip angle(rad)
β_2	Rear sideslip angle (rad)
δ	Front mean steering angle (rad)
ΔC_{a1}	Front adaptive cornering stiffness ($N\,rad^{-1}$)
ΔC_{a2}	Rear adaptive cornering stiffness ($N\,rad^{-1}$)
$\dot{\psi}$	Yaw rate ($rad\,s^{-1}$)
γ_x	Longitudinal accelerations ($m\,s^{-2}$)
γ_y	Lateral accelerations ($m\,s^{-2}$)

Table B2
Nomenclature (second part).

Symbol	Description
x, y	Longitudinal and lateral vehicle positions (m)
$\mathbf{X}$, $\mathbf{Y}$	SMO, state, measurement vectors
$\widehat{\mathbf{x}}$	SMO, state estimation vector
$\widetilde{\mathbf{X}}$	SMO, vector of state estimation errors
$\widehat{\mathbf{y}}$	SMO, vector of measurement estimates
$\widetilde{\mathbf{Y}}$	SMO, vector of measurement estimation errors
$\mathbf{X}'$, $\mathbf{U}'$, $\mathbf{Y}'$	EKF, state, input, measurement vectors
$\widehat{\mathbf{x}}'$	EKF, state estimation vector
$\widehat{\mathbf{y}}'$	EKF, vector of measurement estimates

References

Arndt, C., & Karidas, J. (2006). Estimation of tire–road contact for integrated control applications in current vehicles. In *Proceedings of the IEEE conference on control application*, CCA, Munich, Germany (pp. 2784–2789).

Baffet, G. (2007). *Development and experimental evaluation of tire–road force observers of a vehicle*. Ph.D. thesis, Universite de Technologie de Compiegne, Compiegne, France.

Baffet, G., Stephant, J., & Charara, A. (2007). Experimental evaluation of tire–road forces and sideslip angle observers. In *Proceedings of the IEEE European control conference*, ECC, Kos, Greece.

Burckhardt, M. (1993). *Fahrwerktechnik: Radschlupfregelsysteme*. Vogel.

Canudas-De-Wit, C., Tsiotras, P., Velenis, E., Basset, M., & Gissinger, G. (2003). Dynamic friction models for road/tire longitudinal interaction. *Vehicle System Dynamics*, *39*, 189–226.

Drakunov, S., & Utkin, V. (1995). Sliding mode observers. In *IEEE conference on decision and control* (pp. 3376–3379).

Gustafsson, F. (1997). Slip-based tire–road friction estimation. *Automatica*, *33*(6), 1087–1099.

Han, K. J., Kim, I. K., Jo, H. Y., & Huh, K. S. (2009). Development and experimental evaluation of an online estimation system for vehicle mass. *Proceedings of the Institution of Mechanical Engineers*, *Part D: Journal of Automobile Engineering*, *223*(2), 167–177, ISSN 0954-4070.

Hsu, Y. H. J., & Gerdes, J. C. (2006). A feel for the road: A method to estimate tire parameters using steering torque. In *Proceedings of the eighth international symposium on advanced vehicle control*, AVEC, Taipei, Taiwan (pp. 835–840).

Kalman, R. E. (1960). A new approach to linear filtering and prediction problems. *Transactions of the ASME—Journal of Basic Engineering, Série D*, *82*, 35–45.

Kiencke, U., & Daib, A. (1997). Observation of lateral vehicle dynamics. *Control Engineering Practice*, *5*(8), 1145–1150.

Kiencke, U., & Nielsen, L. (2000). *Automotive control system*. Berlin: Springer.

Kim, J. (2009). Identification of lateral tyre force dynamics using an extended Kalman filter from experimental road test data. *Control Engineering Practice*, *17*(3), 357–367.

Lakehal-ayat, M., Tseng, H. E., Mao, Y., & Karidas, J. (2006). Disturbance observer for lateral velocity estimation. *Proceedings of the eighth international symposium on advanced vehicle control AVEC*, Taipei, Taiwan (pp. 889–894).

Lechner, D. (2002). *Analysis of road vehicle dynamics*: *Development of a methodology applied to primary safety*. Ph.D. thesis, Science of Mechanics, Ecole Centrale de Lyon (defended on June 24th 2002).

Levant, A. (1993). Sliding order and sliding accuracy in sliding mode control. *International Journal of Control*, *58*(6), 1247–1263.

Mohinder, S. G., & Angus, P. A. (1993). *Kalman filtering theory and practice*. Englewood Cliffs, NJ: Prentice-Hall.

Nijmeijer, H., & Van der Schaft, A. J. (1990). *Nonlinear dynamical control systems*. Berlin: Springer.

Ono, E., Asano, K., Sugai, M., Ito, S., Yamamoto, M., Sawada, M., et al. (2003). Estimation of automotive tire force characteristics using wheel velocity. *Control Engineering Practice*, *11*(12), 1361–1370.

Pacejka, H. B., & Bakker, E. (1991). The magic formula tyre model. In *Proceedings of first international colloquium on tyre models for vehicle dynamics analysis (pp. 1–18)*.

Rabhi, A., M'Sirdi, N. K., Zbiri, N., & Delanne, Y. (2005). Vehicle–road interaction modelling for estimation of contact forces. *Vehicle System Dynamics 43*(Suppl.), 403–411.

Ray, L. (1997). Nonlinear tire force estimation and road friction identification: Simulation and experiments. *Automatica*, *33*(10), 1819–1833.

Segel, M. L. (1956). Theoretical prediction and experimental substantiation of the response of the automobile to steering control. In *Proceedings of automobile division of the institute of mechanical engineers* (Vol. 7, pp. 310–330).

Slotine, J., Hedrick, J., & Misawa, E. (1987). On sliding observer for nonlinear systems. *Journal of Mathematical Systems, Estimation and Control*, *109*, 245–259.

Stephant, J., Charara, A., & Meizel, D. (2007). Evaluation of a sliding mode observer for vehicle sideslip angle. *Control Engineering Practice*, *15*, 803–812.

Tanelli, M., Savaresi, S., & Cantoni, C. (2006). Non-local extremum seeking control for active braking control systems. In *Proceedings of the IEEE conference on control application*, CCA, Munich, Germany (pp. 891–896).

Ungoren, A. Y., Peng, H., & Tseng, H. E. (2004). A study on lateral speed estimation methods. *International Journal of Vehicle Autonomous Systems*, *2*(1/2), 126–144.

Wesemeier, D., & Isermann, R. (2009). Identification of vehicle parameters using stationary driving maneuvers. *Control Engineering Practice* doi:10.1016/j.conengprac.2008.10.008.